Digital Object Identifier 10.1109/ECCE44975.2020.9235338

2020 IEEE Energy Conversion Congress and Exposition (ECCE)

State-feedback-based Low-Frequency Active Damping for VSC Operating in Weak-Grid Conditions

Federico Cecati

Rongwu Zhu

Marco Liserre

Xiongfei Wang

State-feedback-based Low-Frequency Active Damping for VSC Operating in Weak-Grid Conditions

Federico Cecati*, Rongwu Zhu*, Marco Liserre*, Xiongfei Wang†
*Chair of Power Electronics, *Christian-Albrechts-Universität* Kiel, Germany
†Department of Energy Technology, *Aalborg University*, Aalborg, Denmark
fc@tf.uni-kiel.de, rzh@tf.uni-kiel.de, ml@tf.uni-kiel.de, xwa@et.aau.dk

***Abstract*—Voltage source converters (VSCs) are nowadays widely integrated in the power grid, nevertheless they can induce low frequency stability problems under weak grid conditions. The interaction of PLL, dc-link voltage control, and ac voltage control generates a positive feedback which threatens the power system stability. The existing researches mainly focus on modeling strategies and stability analyses tools, however still few studies dealt with active damping in the low frequency range. In this paper, a nonlinear state space model of a VSC is presented and linearized around the operating point. From the model, a linear state feedback control law is designed and incorporated in the dc-link and ac voltage control in order to increase the system damping. Eigenvalue analysis is used to investigate the performance of the proposed controller. The simulation results based on a 2 MW grid connected wind generation unit, clearly show the effectiveness of the proposed solution. Experimental results with a 4 kW scaled-down setup validate the analytic and simulation results.**

***Index Terms*—Low Frequency Stability, Voltage Source Converter, Active Damping**

I. Introduction

The evolution of the transmission and distribution grid towards a power converter dominated network brings instability problems in various frequency ranges [1]–[3]. Low frequency stability problems in modern power system have been investigated in literature, and several possible causes have been identified [4]–[10]. The constant power characteristic of the power converters results in a negative resistance behavior, which deteriorates the grid stability [11], [12]. The interactions between PLL, dc-link and ac voltage control have been reported as a major cause of instability in the low frequency range [4], [7]. The instability phenomena becomes more severe under weak grid condition, when the distributed generator is far away from the main grid or with high penetration of power electronics in the grid [4].

The abovementioned instability problems have been modeled and analyzed under different points of view in literature. Nevertheless, active damping strategies to concurrently address all of them are still under development. The research [12] used the ac voltage filtered through a bandpass filter as feedback inside the dc-link voltage control to increase the damping. However, since only a variable is used as feedback, the resulting damping action is limited. The publication [13] proposed a 2 degrees of freedom Active Damping (AD) for VSC operating in autonomous microgrid. However, the dc-link dynamics is not considered in the paper.

In this paper, a nonlinear state-space model of a grid-connected voltage source converter (VSC) is derived, and linearized around the operating point [14]. From the obtained linear state-space model, a state-feedback based AD is designed through eigenvalue placement method [15], [16]. The eigenvalue placement is realized through a systematic and straightforward procedure, which aims to make the control design almost completely machine-based, avoiding laborious eigenvalue placement designs. An additional parameter σ is included in the control law to regulate the damping intensity and provide an additional degree of freedom to the controller.

The rest of the paper is structured as follows: Section 2 presents the system under consideration and its state space model, Section 3 describes the proposed state-feedback controller with the eigenvalue placement algorithm, Section 4 provides the simulation results, Section 5 shows the experimental results and Section 6 deals with the conclusions.

II. System Description and Modeling

The schematic of the grid-connected VSC under analysis is depicted in Fig. 1(a). The current generator i_{dc} represents the primary energy source, i.e. the photovoltaic module or the wind turbine. The converter implements the PI controller for the dc-link voltage, the PI controller for the ac voltage and a synchronous reference frame phase locked loop (SFR-PLL) for the synchronization. The current control is realized through a PI regulator in the synchronous reference frame [2]. The

The authors gratefully acknowledge funding by German Federal Ministry for Economic Affairs and Energy within the research project "Add-On" (0350022B) and by Gesellschaft für Energie und Klimaschutz Schleswig-Holstein GmbH (EKSH) doctoral studies grant.

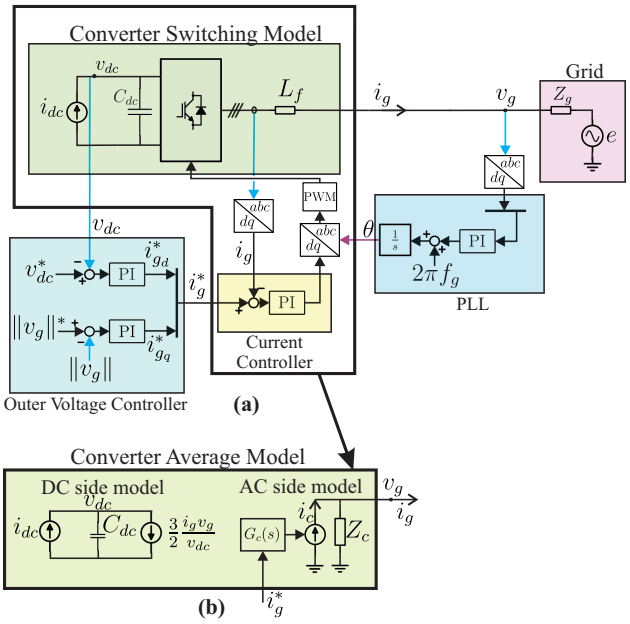

Figure 1: The three-phase grid connected voltage source converter under analysis. (a) The switching model and the control loop, (b) the average model of the converter.

converter is plugged to the grid through an impedance Z_g, which is composed of a resistive component R_g and an inductive component L_g.

Since this paper is focused on the low frequency stability issues, the converter hardware part modeling is realized through an average model shown in Fig. 1(b). The dc side model is realized according to the active power balance equation [2]. The ac side model is realized through a current source i_c, and a parallel impedance Z_c representing the current loop equivalent virtual impedance [17]. The derived impedance model is then converted in state-space form.

The derivation of the ac side state-space model starts from the expression of the injected current i_g in the ac side in the frequency domain.

$$i_g = G_c(s)i_g^* + Y_c(s)v_g \tag{1}$$

being $Y_c(s) = \frac{1}{Z_c(s)}$. The transfer functions in (1) are defined as:

$$\begin{cases} G_c(s) = \dfrac{K_p s + K_i}{L_f s^2 + K_p s + K_i} \\ Y_c(s) = \dfrac{s}{L_f s^2 + K_p s + K_i} \end{cases} \tag{2}$$

which can be approximated to the first order as:

$$\begin{cases} G_c(s) = \dfrac{1}{1 + \frac{L_f}{K_p}s} \\ Y_c(s) = \dfrac{\frac{s}{K_p}}{1 + \frac{K_i}{K_p}s} \end{cases} \tag{3}$$

Considering the approximation in (3), the model (1) can be expressed in state-space form as:

$$\begin{cases} \dot{v}_{cc} = K_i i_c - K_i i_g \\ \dot{i}_c = -\frac{K_p}{L_f} i_c + \frac{K_p}{L_f} i_g^* \\ v_g = K_p\left(i_c - i_g\right) + v_{cc} \end{cases} \tag{4}$$

Starting from the ac side model in (4), adding the dc side, the outer loops and the grid model, the proposed state-space nonlinear model of the whole system is derived:

$$\begin{cases} \dot{i}_c = -\frac{K_p}{L} i_c + \frac{K_p}{L} i_g^* \\ \dot{v}_{dc} = -\frac{3}{2}\frac{1}{C_{dc}}\frac{v_g \cdot i_g}{v_{dc}} + \frac{1}{C_{dc}} i_{dc} \\ \dot{\Phi}_{dc} = v_{dc} - v_{dc}^* \\ \dot{\Phi}_g = v_g^* - \sqrt{v_g \cdot v_g} \\ \dot{\delta} = \begin{pmatrix} 0 & K_{p,PLL} \end{pmatrix} v_g + K_{i,PLL}\Phi_q \\ \dot{\Phi}_q = \begin{pmatrix} 0 & 1 \end{pmatrix} v_g \\ \dot{v_{cc}} = -K_i i_g + K_i i_c \\ \dot{i}_g = \frac{R_g}{L_g} i_g - \Omega i_g + \frac{1}{L_g} v_g - T(\delta)e \end{cases} \tag{5}$$

with

$$\begin{cases} \Omega = \begin{pmatrix} 0 & -2\pi 50 \\ 2\pi 50 & 0 \end{pmatrix} \\ T(\delta) = \begin{pmatrix} \cos\delta & \sin\delta \\ -\sin\delta & \cos\delta \end{pmatrix} \\ i_g^* = \begin{pmatrix} K_{p,DC}(v_{dc} - v_{dc}^*) + K_{i,DC}\Phi_{dc} \\ K_{p,AC}(v_g^* - \sqrt{v_g \cdot v_g}) + K_{i,AC}\Phi_g \end{pmatrix} \end{cases} \tag{6}$$

In (5) the state is defined as $x = \begin{pmatrix} i_c & v_{dc} & \Phi_{dc} & \Phi_g & \delta & \Phi_q & v_{cc} & i_g \end{pmatrix}$ where Φ_{dc}, Φ_g and Φ_q are the integral states for the dc-link, ac voltage controllers and PLL respectively, and v_{cc} is an auxiliary state variable to express v_g. The disturbance input is defined as $d = \begin{pmatrix} i_{dc} & e \end{pmatrix}$ while the reference input is defined as $r = \begin{pmatrix} v_{dc}^* & v_g^* \end{pmatrix}$. For the linearization, the operating point is defined by constant values d_e and r_e of the inputs, and the nonlinear vectorial differential equation (5), expressed the form $\dot{x} = f(x, d_e, r_e)$, is integrated in order to compute the equilibrium state x_e. Once it is derived, the Jacobian matrices are computed and evaluated in the equilibrium point. The resulting linearized system has the form

$$\dot{x} = Ax + Fd + Gr \tag{7}$$

with

$$\begin{cases} A = \left.\dfrac{\partial f}{\partial x}\right|_{x=x_e, d=d_e, r=r_e} \\ F = \left.\dfrac{\partial f}{\partial d}\right|_{x=x_e, d=d_e, r=r_e} \\ G = \left.\dfrac{\partial f}{\partial r}\right|_{x=x_e, d=d_e, r=r_e} \end{cases} \tag{8}$$

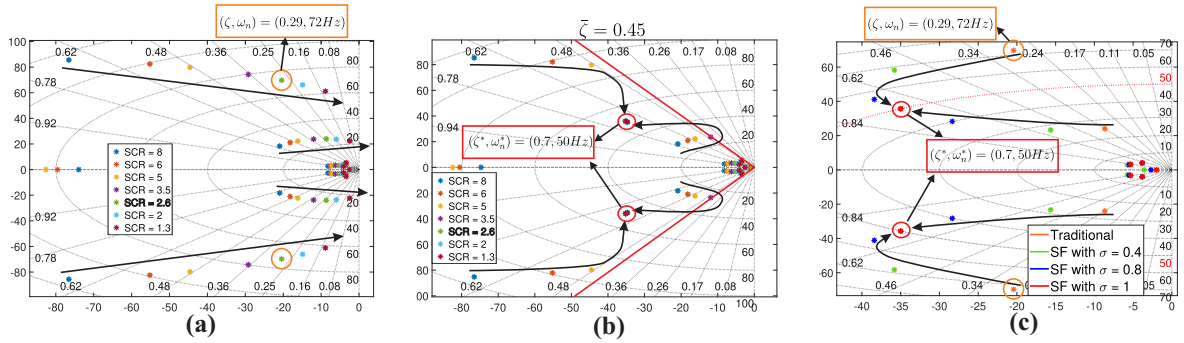

Figure 2: The eigenvalue analysis of the grid connected VSC depending on the grid SCR. (a) Traditional PI controller (b) State-feedback AD controller with $\sigma = 1$ (the red lines represent the critical damping $\bar{\zeta}$). (c) The eigenvalue shift respect to the coefficient σ.

III. The State-Feedback Control

The proposed nonlinear model (5) is used to model a VSC-based wind generation unit with a power rating of 2 MW. Based on the state-space model (8), the eigenvalue analysis of the VSC connected to the grid as in Fig. 1(a) is realized for different short circuit ratio (SCR) values, as shown in Fig. 2(a). From this analysis it emerges as values of the SCR lower than 2.6 are associated with low damped dynamics ($\zeta < 0.3$), in accordance with other papers in literature [1], [4]. That represents a hazard for the grid stability.

The target of this paper is to address the stability problems highlighted in Fig. 2(a) through a state-feedback based active damping solution. That is realized through the introduction a feedback loop, denominated with u, directly in the current controller reference as in Fig. 3. The blue arrows in Fig. 3 indicate the state variables physically measured. The orange arrows indicate non-physical state variables obtained though operations on the existing variables.

The feedback signal u is included in the state-space model (5) by modifying the first differential equation as follows:

$$\dot{i}_c = -\frac{K_p}{L} i_c + \frac{K_p}{L}\left(i_g^* + u\right) \tag{9}$$

Consequently, the matrix B can be computed as

$$B = \left.\frac{\partial f}{\partial u}\right|_{x=x_e, d=d_e, r=r_e} \tag{10}$$

similar to (8). The model in (8) becomes:

$$\dot{x} = Ax + Bu + Fd + Gr \tag{11}$$

and the state feedback design can be done on the linearized model $\dot{x} = Ax + Bu$, considering Fd and Gr as disturbances.

The state-feedback gain matrix K is computed through eigenvalue placement procedure [18]. However, the choice of the vector of the desired eigenvalues $\bar{P}$ which reaches a good compromise between system damping, system dynamic response and control effort remain still an open issue.

In this paper, an algorithm for the choice of $\bar{P}$ is proposed, and graphically explained in Fig. 4. The eigenvalues which do not meet the specification defined by the minimum allowed damping $\bar{\zeta}$ and the minimum allowed natural pulsation $\bar{\omega_n}$, are moved to a region defined by ζ^* and ω_n^*; the eigenvalues which do meet the specification, are not moved. The functioning of the algorithm can be better understood from Fig. 2(b), in which $\bar{\zeta} = 0.45$ and $\bar{\omega_n} = 50$ rad/s. For SCRs > 4 all the eigenvalues of the system do respect the specification, thus are not moved. For SCRs ≤ 4 the low damped eigenvalues are moved to a desired position determined by $\zeta^* = \frac{1}{\sqrt{2}}$ and $\omega_n^* = 50$rad/s. The aim of the proposed algorithm is to make a systematic choice of the matrix K, and to use a coefficient σ shown in Fig. 3 to regulate the damping feedback strength.

The damping regulation capability of σ is shown through eigenvalue analysis in Fig. 2(c). By increasing the value of σ, the eigenvalues approach the desired point defined by $\zeta^* = \frac{1}{\sqrt{2}}$ and $\omega_n^* = 50$rad/s. This demonstrates how σ can regulate the damping strength. Overall, the proposed control design includes two steps, the first is the computation of optimal damping feedback matrix K with the systematic procedure of Fig. 4, and as second is the regulation of the damping strength through the coefficient σ.

Table I: The value of ρ for different grid SCRs.

Grid SCR	ρ
8	1.08
6	1.28
5	1.05
3.5	1.88
2.6	4.59
2	4.61
1.3	3.33

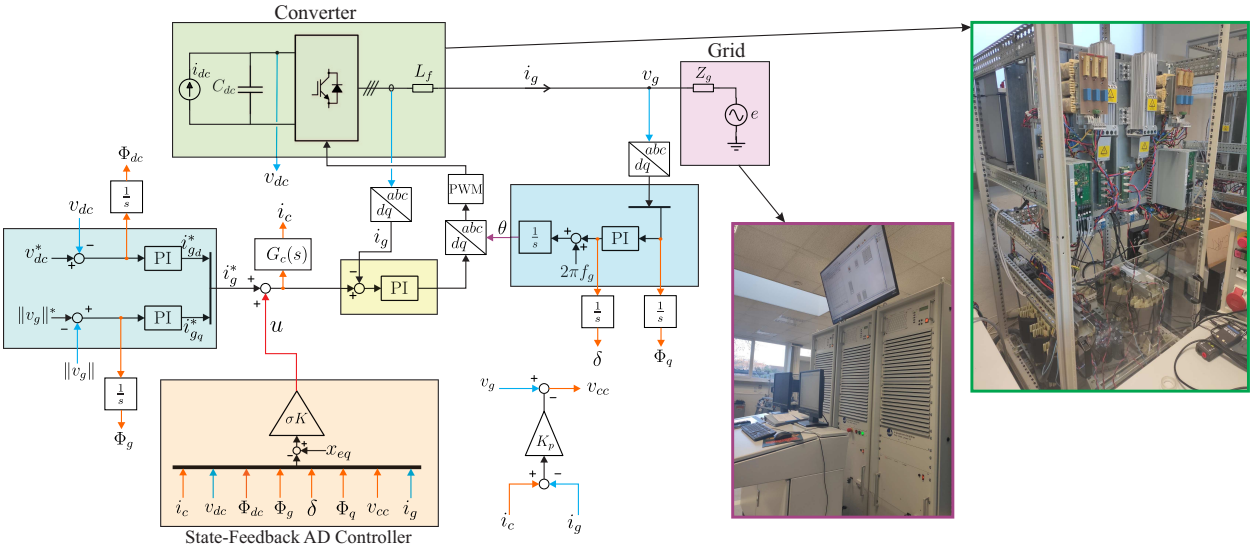

Figure 3: The implementation scheme of the proposed state-feedback AD controller. In the right, the back to back converter and the power amplifier used for the experimental results.

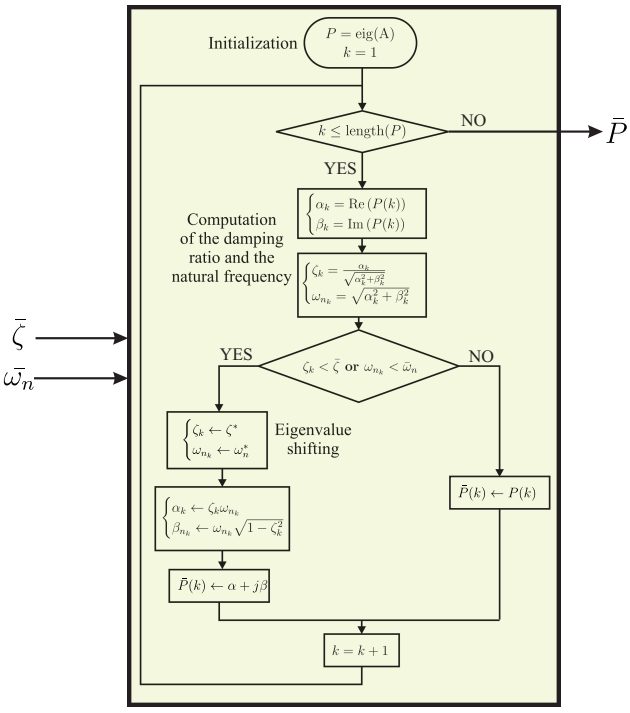

Figure 4: The flowchart of the proposed eigenvalue placement algorithm.

IV. Simulation Results

The proposed state-feedback controller is implemented in a simulation of a 2 MW wind turbine with a VSC as interface with the grid. The SCR of the considered grid is equal to 2.6, represented by the green eigenvalues in Fig. 2. A symmetrical voltage sag of 0.35 p.u. with a phase jump of 18 degrees is simulated at time 1.3 s, and the behavior of the dc-link voltage, PCC voltage and injected current is depicted in Fig. 5 with respect to the coefficient σ. It can be noticed in Fig. 5 that, in the case $\sigma = 0$, corresponding to no active damping case, severe oscillations are present in the VSC currents and voltages, which may threaten the grid stability. When $\sigma = 0.4$, the AD feedback shifts to the left the critical eigenvalues, as shown in Fig. 2(c), resulting in more damped oscillations and higher stability margins. The situation is different for $\sigma = 0.8$. In the first fractions of seconds after the sag, the oscillations on currents and voltages are more damped respect to the case of $\sigma = 0.4$. Nevertheless, at time $t = 1.4s$ an overmodulation phenomena occurs, causing a distortion in the injected current. The phenomena can be noticed in the VSC injected current in Fig. 5(b), and is clearly shown in Fig. 5(c). Nevertheless, the occurrence of the overmodulation could not be presaged from the linear eigenvalue analysis in Fig. 2, since it is a nonlinear phenomena, due to the too high control effort needed to damp the oscillations.

The needed control effort is dependent on many variables, including the grid SCR, the dc-link capacitor, VSC power rating and current loop bandwidth, thus difficult to quantify. However, with the help of the functional analysis, a parameter

$$\rho = \sigma \frac{\|K\|_2}{\|x_e\|_2} \tag{12}$$

which is the L^2-norm of the matrix K normalized respect to the equilibrium state x_e norm, can be defined. It represents the generalized normalized gain of the damping feedback, and provides an absolute measure

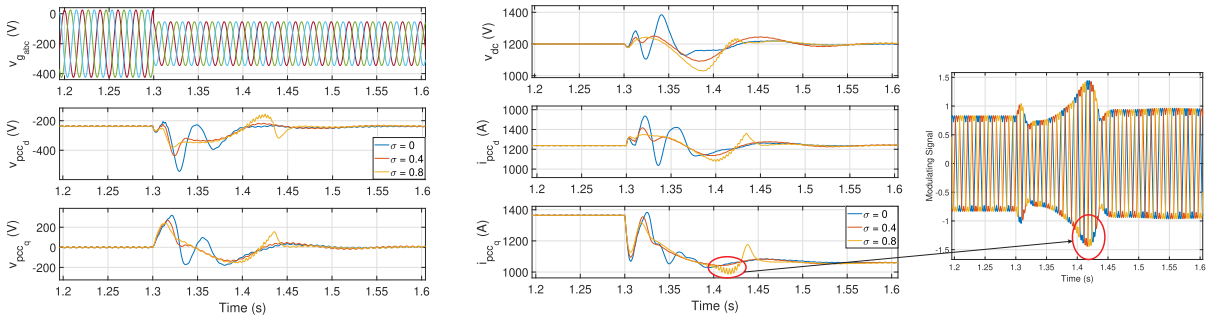

Figure 5: The VSC dynamic response to a symmetrical voltage sag for different values of σ. (a) The grid voltage and the PCC voltage. (b) The dc-link voltage and the injected current. (c) The modulation index in the case $\sigma = 0.8$

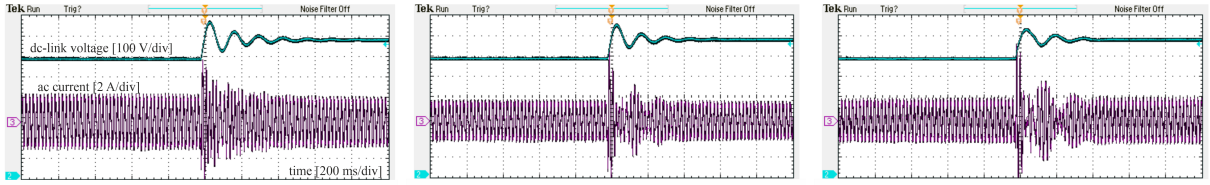

Figure 6: The experimental results in three different cases. (a) Traditional PI controller, (b) state-feedback controller with $\sigma = 0.4$, (c)state-feedback controller with $\sigma = 0.8$.

of the damping strength. The dependence of ρ on the SCR is shown in Table I. It is clear from the table, as with lower SCR the control effort needed to damp the system is higher, and ρ is higher. However, when the SCR is very low, the grid impedance is very high, and even if the oscillation are big, less current is necessary to induce a desired voltage drop in the PCC. That is the reason why for SCR=1.3 less control effort respect to SCR=2 is needed.

From empirical studies, a value of ρ less than 2 is recommended to obtain good performances and to not encounter the overmodulation phenomena. The parameter ρ in the case study is equal to 4.59 with $\sigma = 1$. Reducing σ to 0.4 allows to reduce ρ until 1.84, resulting in lower control effort and no overmodulation, as shown in Fig. 5.

V. Experimental Results

The proposed controller is implemented in a Microlabbox-controlled VSC connected to a grid with SCR equal to 4. A increase from 600 V to 700 V is given to the dc-link voltage reference, and the dynamic behavior is depicted in Fig. 6 under different values of σ, analogously to Fig. 5. In Fig. 6, increasing values of σ results in lower overshoot and higher damping of the dc-link voltage, in accordance with the analysis in Fig. 2; no overmodulation phenomena can be noticed, in this case. Indeed, in this case study the value of ρ for $\sigma = 1$ is 0.96, much lower respect to the case of the previous section ($\rho = 4.59$). Indeed, the SCR of the grid considered in the experimental results (SCR=4) is significantly higher respect to the one considered in the simulation (SCR=2.6), thus less damping control effort is needed. Therefore, $\sigma = 0.8$ is a good value for the AD implemented in the considered experimental setup.

VI. Conclusions

The proposed state-feedback controller has the capability to damp the low frequency dynamics in voltage source converters connected to weak grid. The simulation and experimental results confirm the analytic results showing high damping performance and lower overshoot of the state-feedback respect to the PI traditional controller. However, a too strong damping action can result in converter overmodulation; the index ρ is defined to quantify the control effort. The parameter σ allows to regulate the control effort and, in case of a too high ρ, it can be reduced in order to avoid overmodulation phenomena. Both the simulations and the experimental results confirm as through the regulation of σ a good compromise between damping capability and control effort can be achieved.

References

[1] X. Wang and F. Blaabjerg, "Harmonic stability in power electronic-based power systems: Concept, modeling, and analysis," *IEEE Trans. Smart Grid*, vol. 10, no. 3, pp. 2858–2870, May 2019.

[2] R. Teodorescu, M. Liserre, and P. Rodriguez, *Grid converters*

for photovoltaic and wind power systems. John Wiley & Sons, 2011, vol. 29.

[3] F. Blaabjerg, Y. Yang, D. Yang, and X. Wang, "Distributed power-generation systems and protection," *Proc. IEEE*, vol. 105, no. 7, pp. 1311–1331, 2017.

[4] Y. Huang *et al.*, "Modeling of vsc connected to weak grid for stability analysis of dc-link voltage control," *IEEE Trans. Emerg. Sel. Topics Power Electron.*, vol. 3, no. 4, pp. 1193–1204, 2015.

[5] N. Pogaku, M. Prodanovic, and T. C. Green, "Modeling, analysis and testing of autonomous operation of an inverter-based microgrid," *IEEE Trans. Power Electron.*, vol. 22, no. 2, pp. 613–625, 2007.

[6] M. Rasheduzzaman *et al.*, "Reduced-order small-signal model of microgrid systems," *IEEE Trans. Sustain. Energy*, vol. 6, no. 4, pp. 1292–1305, Oct. 2015.

[7] H. Yuan, X. Yuan, and J. Hu, "Modeling of grid-connected vscs for power system small-signal stability analysis in dc-link voltage control timescale," *IEEE Trans. Power Syst.*, vol. 32, no. 5, pp. 3981–3991, 2017.

[8] X. Wang, F. Blaabjerg, and W. Wu, "Modeling and analysis of harmonic stability in an ac power-electronics-based power system," *IEEE Trans. Power Electron.*, vol. 29, no. 12, pp. 6421–6432, 2014.

[9] D. Dong, B. Wen, D. Boroyevich, P. Mattavelli, and Y. Xue, "Analysis of phase-locked loop low-frequency stability in three-phase grid-connected power converters considering impedance interactions," *IEEE Trans. Ind. Electron.*, vol. 62, no. 1, pp. 310–321, 2015.

[10] F. Cecati, M. Andresen, R. Zhu, Z. Zou, and M. Liserre, "Robustness analysis of voltage control strategies of smart transformer," in *IECON 2018 - 44th Annual Conference of the IEEE Industrial Electronics Society*, Oct. 2018, pp. 5566–5573.

[11] N. Bottrell, M. Prodanovic, and T. C. Green, "Dynamic stability of a microgrid with an active load," *IEEE Trans. Power Electron.*, vol. 28, no. 11, pp. 5107–5119, Nov. 2013.

[12] K. M. Alawasa, Y. A. I. Mohamed, and W. Xu, "Active mitigation of subsynchronous interactions between pwm voltage-source converters and power networks," *IEEE Trans. Power Electron.*, vol. 29, no. 1, pp. 121–134, 2014.

[13] A. Kahrobaeian and Y. A. I. Mohamed, "Analysis and mitigation of low-frequency instabilities in autonomous medium-voltage converter-based microgrids with dynamic loads," *IEEE Transactions on Industrial Electronics*, vol. 61, no. 4, pp. 1643–1658, 2014.

[14] H. K. Khalil and J. W. Grizzle, *Nonlinear systems*. Prentice hall Upper Saddle River, NJ, 2002, vol. 3.

[15] J. Kautsky, N. K. Nichols, and P. Van Dooren, "Robust pole assignment in linear state feedback," *Int. J. Control*, vol. 41, no. 5, pp. 1129–1155, 1985.

[16] G. F. Franklin, J. D. Powell, A. Emami-Naeini, and J. D. Powell, *Feedback control of dynamic systems*. Addison-Wesley Reading, MA, 1994, vol. 3.

[17] L. Harnefors, M. Bongiorno, and S. Lundberg, "Input-admittance calculation and shaping for controlled voltage-source converters," *IEEE Trans. Ind. Electron.*, vol. 54, no. 6, pp. 3323–3334, Dec. 2007.

[18] J. Kautsky, N. K. Nichols, and P. Van Dooren, "Robust pole assignment in linear state feedback," *International Journal of control*, vol. 41, no. 5, pp. 1129–1155, 1985.